AU/AFF/NNN/2013-XX

AIR FORCE FELLOWS

AIR UNIVERSITY

NUMERICAL SIMULATION OF CRATERING EFFECTS IN ADOBE

By

Jeremy R. Peña, DAF

A Research Report Submitted to the Air Force Fellows
in Partial Fulfillment of the Graduation Requirements

Advisors:
Larry A. Schoof
Stephen Attaway
Aaron Brundage

Weapon Intern Program

"Sandia National Laboratories is a multi-program laboratory managed and operated by Sandia Corporation, a wholly owned subsidiary of Lockheed Martin Corporation, for the U.S. Department of Energy's National Nuclear Security Administration under contract DE-AC04-94AL85000."

Maxwell Air Force Base, Alabama

July 2013

Disclaimer

The views expressed in this academic research paper are those of the author(s) and do not reflect the official policy or position of the US government or the Department of Defense. In accordance with Air Force Instruction 51-303, this research paper is not copyrighted but is the property of the United States government.

Contents

Page

ILLUSTRATIONS

Page

TABLES

Page

Acknowledgments

I would like to thank Stephen Attaway, Aaron Brundage, and John Korbin for their tireless guidance and support to complete such research. This paper would not exist without their help. Thanks also goes out to Richard Neiser, William Tedeschi, and Larry Schoof for taking me on as an intern and training to use CTH, a Sandia National Laboratories developed shock physics code that is widely used across the DOE and DoD. Last but not least I would like to thank the Air Force Fellows program for the opportunity to expand my knowledge in support of this country's security.

Abstract

This paper outlines a new simplified approach to developing a material model for adobe. The approach is to fit the equation of state (E0S) using a Mie-Grüneisen (MGR) analytical model with a P-Alpha compaction law, and to fit the pressure-dependent yield surface with the Geological Yield Surface (GEO) modeled in CTH using well characterized adobe. By identifying key parameters that governed material response, this simplified modeling approach aimed to increase the understanding of the shock compaction and compression behavior of adobe.

The new simplified model for adobe represented in this paper replicated the features of past experimental penetration data. At low velocities the penetration behavior of steel spheres into adobe is captured by Stokes law, where the drag coefficient is inversely proportional to the Reynolds number. Each inherently different adobe material investigated had a separate linear region with the slope equal to the inverse of the coefficient of drag multiplied by impact velocity. A transition region following the Stokes region was identified in each adobe material, where the penetration depth was constant with increasing impact velocity. This penetration depth limit was shown to be dependent upon the yield strength of the adobe and inversely proportional to the initial density.

Finally, examining the sensitivity of the penetration depth to the key model parameters, the material model for adobe was adjusted to provide the best fit to the experimental penetration data. In addition, a simplified water content, or initial saturation of the adobe, was introduced as another relevant parameter to characterize the response. Using this simple material model for adobe, validated with experimental penetration data, the response of adobe targets to hypervelocity impact of a variety of projectile types can be reliably predicted.

Chapter 1

Introduction

> *Before I came here I was confused about this subject. Having listened to your lecture I am still confused, but on a higher level.*
>
> —Enrico Fermi

There has been a shift of focus in the shock physics community in the last few years on high velocity impacts and penetration of non-porous materials (i.e. steel, aluminum) to that of adobe or other more porous materials. This is a study on numerical modeling and simulation of high velocity penetrations into adobe using the Sandia National Laboratory shock physics code, CTH. Defining the equation of state and yield parameters for the simulations is provided by static mechanical tests on adobe specimens. Simulation results are compared to past test and computational data based upon different equations of state and material strength models. To conclude several parameters that define the problem are analyzed for sensitivity to the depth of penetration, including the simulation of adding water to the adobe and the effects on crater formation.

Material under Compression

Adobe is typically composed of clay and sand generally used in arid, dry climates. The material is very porous and soft compared to steel or other non-porous materials. Under high pressures the behavior of adobe can be very complex and many factors can contribute to its

response per high velocity impacts. The compaction of adobe can be related similar to soil with voids of water and air. Figure 1 is an example of adobe granules under high pressures.

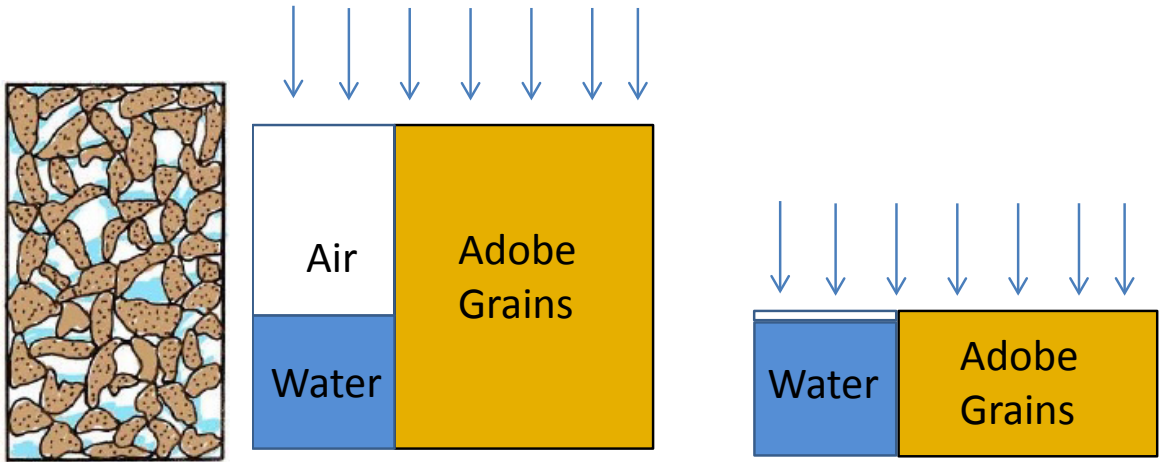

Figure 1: Compression of Adobe Grains with Water and Air Graphic

The initial state of adobe is porous and has an initial density defined as ρ_{oo}. As the adobe is compressed, the voids filled with air start to close and grains of the adobe are shifted, which increases the density of the adobe to a solid (ρ_o). As pressure is increased friction between the grains increases, increasing the shear strength and density of the adobe. Increased fracturing of the granules decreases the volume, increasing the density (ρ_s), in which the change in pressure is much higher than the change in volume and the material is characterized as "*locked-up*". Refer to figure 2 to follow how change in pressure effects the change in density of adobe.

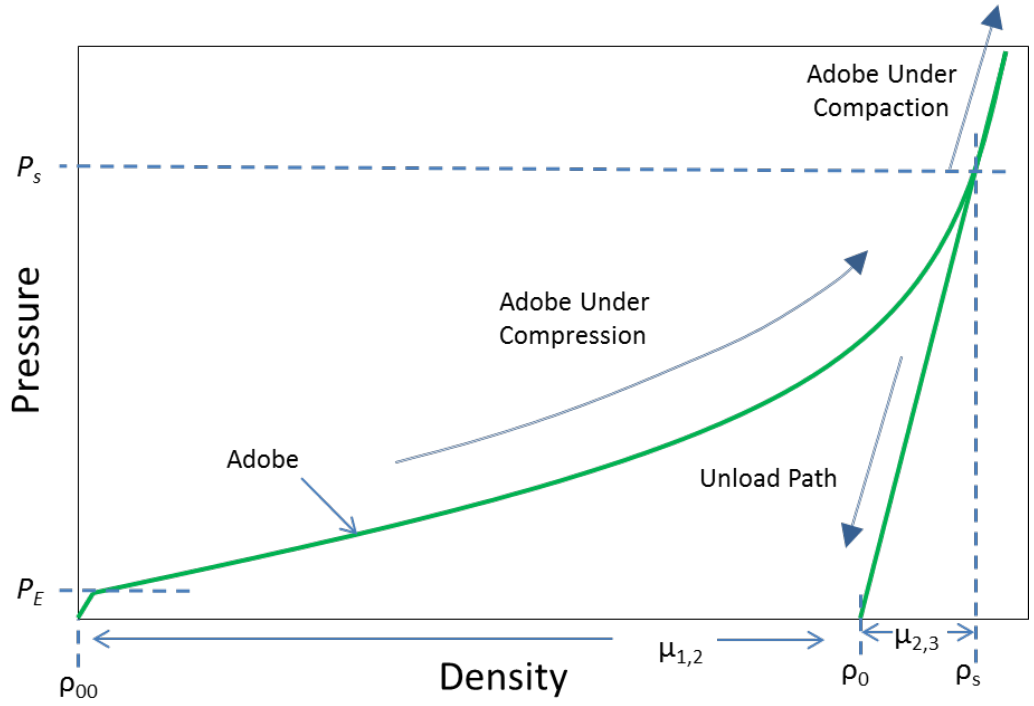

Figure 2: Graphic of Pressure versus Density of Adobe

There are 3 states of adobe as pressure increases beyond elastic pressure (P_E) and continues to compaction pressure (P_s) and beyond. At zero pressure the adobe is at initial density (ρ_{oo}). As pressure increases past the elastic pressure, the adobe continues compression until it reaches compaction pressure where all voids have been closed. Increasing pressure, the change in density is very small compared to the change in pressure and the adobe follows along the compaction curve. The release of pressure the density of the adobe will follow along an unload path as shown in figure 2.

Adobe Compression Data

Two separate reports of compression data on adobe were initially reviewed for this research. In 2008 and in 2012 the U.S. Army Corps of Engineers Engineer Research and Development Center (ERDC), Geotechnical Structures Laboratory (GSL) published studies conducting

mechanical property tests on adobe [1, 9]. Both studies were thorough in characterization of adobe under high pressures however the 2008 study provided strain data at higher pressures with the unload behavior for the adobe. The strain data for the 2012 study was conducted at lower pressures and did not include any unload behavior for the adobe. Shown in figure 3 is the mean normal stress versus percent volumetric strain of the adobe from the ERDC 2008 study under hydrostatic compression up to 400 MPa with unload paths.

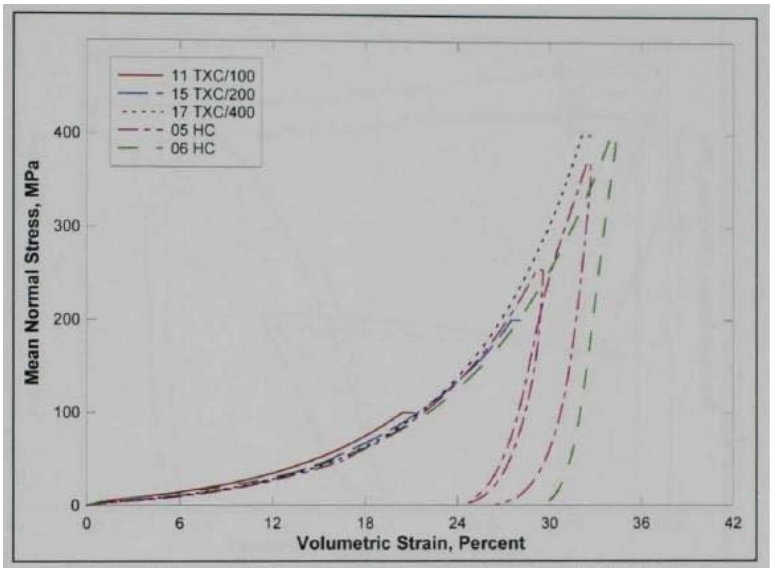

Figure 3: Test Data of Mean Normal Stress versus Percent Volumetric Strain of Adobe under Hydrostatic Compression and Tri-Axial Compression (Williams et al, 2008)

The adobe in the 2008 study had an assumed grain density of 2.51 g/cm^3, a mean water content of 1.67 percent and a mean dry density of 1.599 g/cm^3. There were a total of 46 mechanical property tests conducted on the adobe specimens composed of 75 percent sand, 24 percent clay and 1 percent cement. It was believed at approximately 400 MPa, the adobe just reached complete void closure.

Past Research

A recent literature search on hypervelocity velocity, hard projectiles into adobe brought up only a few articles. In 2011 a team led by A Heine, published experimental results on hypervelocity impacts of spheres and rods into adobe bricks[5]. The team conducted a total of 15 rod penetration experiments and 11 sphere penetration experiments into adobe. The penetration velocities ranged from 500 m/s to 3200 m/s. Heine's adobe had a density of 1.8 g/cm^3, compressive strength of 4 N/mm^2, and sound speed at 1070 m/s.

In 2013 the Army Research Laboratory (ARL), led by C Meyer[8], published a report on modeling and simulation of adobe penetrations with high velocity projectiles of sphere's and rods based upon the test data previously conducted by Heine and his team. Meyer sought to develop high fidelity numerical simulations of adobe penetrations using the Holmquist, Johnson, and Cook (HJC) model in the shock physics code CTH[4]. The basis for defining the parameters for the HJC model was a combination of triaxial test data from the 2008 ERDC study on adobe[9] and test data from Heine[5]. Meyer used the few adobe parameters from Heine's study (initial density, sound speed, and compressive strength) and developed the remaining parameters for the HJC model from the triaxial test data of adobe (grain density, crush pressure, compaction pressure, etc..). Results of the HJC model showed similar characteristics to the test data provided by Heine.

Choosing a Model

Several models were considered when approaching this study of simulating penetrations in adobe with the shock physics code, CTH. Other models such as HJC or Kayenta[2] are very good at simulation a broad class of materials under high pressures but in the end the simplistic

Geological Yield Surface (GEO) strength model with the equation of state (EOS) that included a Mie-Grüneisen (MGR) analytic model with the P-Alpha compaction law was chosen. The GEO model, only needing a few parameters to define the problem, is simpler in comparison to other models but also has its drawbacks. The downside to using the GEO model are the parameters not included other models may have. Other models may require as many as 40 parameters to define a problem but unlike the GEO model, other models may take into account material damage, strain rate hardening, and shear induced dilatation. Using the GEO strength model with the MGR / P-Alpha EOS for adobe, the assumption is made that this simplistic approach can be very useful in simulating crater formation and insensitive to any parameters not defined within the model.

Chapter 2

Development of Material Parameters

The basis for developing the MGR / P-Alpha with GEO simulations of high velocity impacts in adobe first required analysis of adobe through mechanical property tests. As discussed earlier the ERDC 2008 study on adobe provided the necessary data for the EOS and Deviatoric parameters for this study. The next few sections will step through the process of defining the parameters for the simulations for new adobe model called "*GEO*" for short.

Equation of State Parameters

Several parameters for the MGR/P-Alpha model EOS such as initial density, solid density, material sound speed and the shock constant "*s*" were found using lab data shown in figure 3 from the ERDC 2008 study. Extrapolating mean stress and percent volumetric strain data from figure 3, and converting percent strain to normal strain ($\mu_{1,2}$), the solid density (ρ_0) of adobe is found as a function of initial density (ρ_{00}) and strain (equation 1). Initial density as discussed in chapter 1 was found to be 1.599 g/cm^3.

$$\mu_{1,2} = 1 - {}^{\rho_{00}}/_{\rho_0} \qquad \text{Equation 11}$$

Figure 4 is a plot of solid density as a function of pressure of the adobe lab data developed from stress and strain measurements from the adobe hydrostatic and triaxial compression tests.

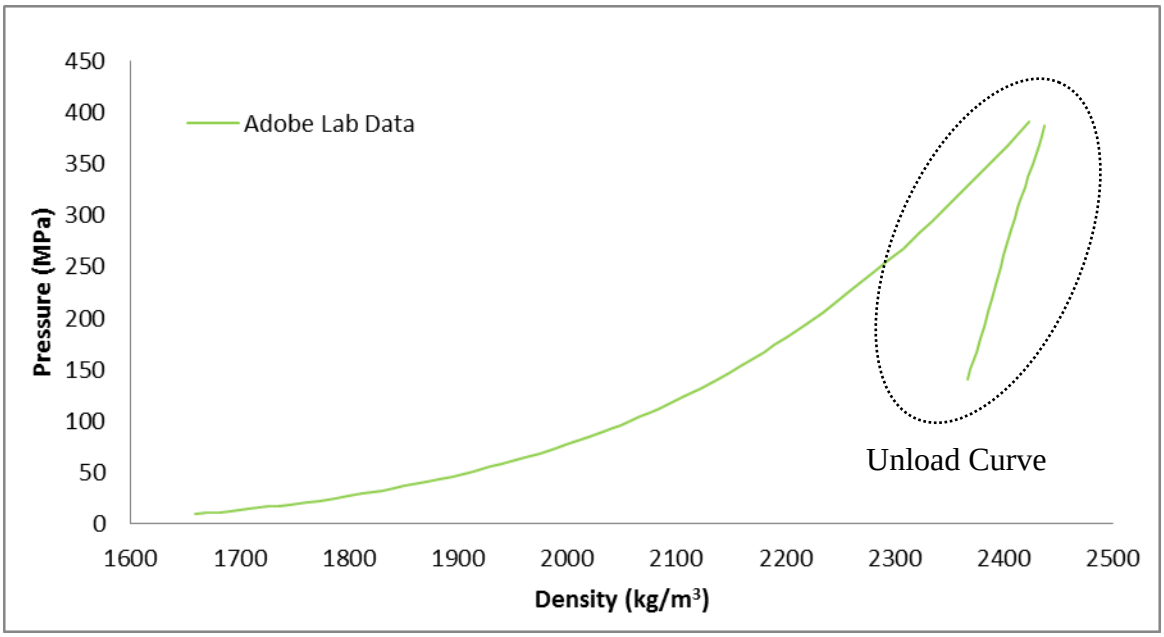

Figure 4: Pressure versus Density Test Data of Adobe with Unload Curve

The unload path, circled in figure 4, gives a good approximation of the slope of the compaction curve, or lock-up, where change in pressure is much larger than change in density. Granite, quartz and tuff were considered as candidates for a rough approximation of the compaction curve under very high pressures. Figure 5 shows the comparisons of the different materials for use as a compaction curve.

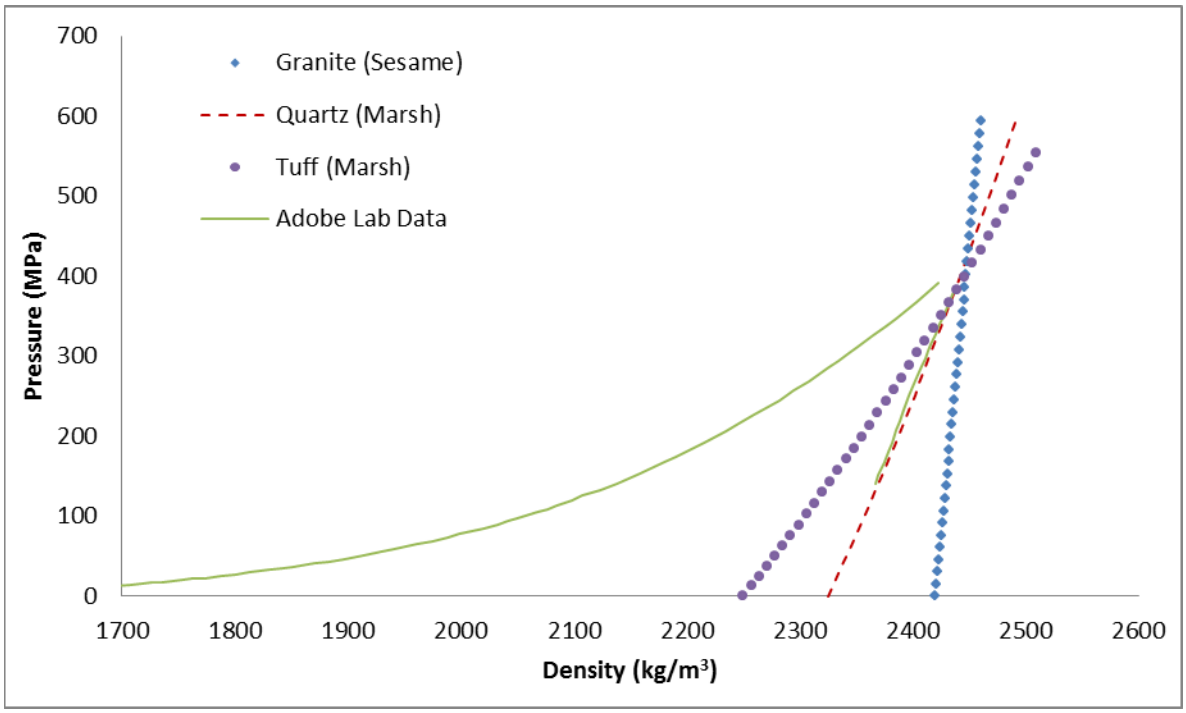

Figure 5: Pressure versus Density Test and Computational Data of Compaction Curves aligned to Adobe Laboratory Data

To plot compaction pressure as a function of density for the various materials shown in figure 5, the sound speed, and shock wave constants were required. Sound speed (C_s) and the shock wave constant "*s*" are found by taking the slope and y-intercept of shock velocity (U) versus particle velocity[3] (u) (i.e. Hugoniot) as shown in equation $U=C_s+su$. Data labeled "Marsh" was pulled from the Los Alamos Series on Dynamic Material Properties by S. P. Marsh[7] and contained test data of shock velocity and particle velocity for those materials. The data labeled "Sesame", found within CTH sesame tables, was processed through a program called "BCAT" producing shock velocity and particle velocity data for that material. Using equation 2 to find compaction pressure as a function of solid density, the "Sesame" and "Marsh" data were plotted as pressure versus density shown in Figure 5.

$$P_s = \frac{C_s^2 \rho_0 \mu}{[1 - s\mu]^2}$$ Equation 22

Quartz showed to be the best fit in matching the slope of the "unload" curve for the Adobe lab data. The y-intercept for the quartz is the solid density (ρ_0) shown to be 2325 kg/m^3. The sound speed and shock constant for quartz are 1746 m/s and 1.63 respectively. Completing the link between the laboratory data and the compaction curve is the P-Alpha curve, discussed in the next section.

P-Alpha Fit

The static mechanical tests of the adobe specimens would only define the parameters up to the largest compressive pressure of the tests. There is a gap between the maximum compressive test data (400 MPa) and the pressures that could occur from high velocity impacts (>>400 MPa). The P-Alpha curve is used to fit across the lab data and compaction curve to approximate the pressure at which the material starts to experience compaction. Equation 3 is the P-Alpha[6] equation where alpha (α) is a function of pressure (P). The compaction pressure (P_s) is the initial pressure at which all void has been removed from the porous material and the grains are under compaction. P_E is the maximum elastic pressure of the material, prior to inelastic behavior of the adobe, which for this case is very small in comparison to P_s. Alpha zero (α_0) is the ratio of the initial density of the adobe (ρ_{00}) and solid density of the adobe (ρ_0) (equation 4). Equation 5 is strain ($\mu_{2,3}$) as a function of the adobe solid density and adobe lock-up density (ρ_s) at high pressures above P_s.

$$\alpha(P) = 1 + (\alpha_0 - 1) \cdot \left[\frac{P_s - P}{P_s - P_E}\right]^N \qquad \text{Equation 3 3}$$

$$\boldsymbol{\alpha_0 = \rho_0 / \rho_{00}} \qquad \text{Equation 44}$$

$$\mu_{2,3} = 1 - \rho_0 / \rho_s \qquad \text{Equation 55}$$

The ERDC study stated the pressure from the compression tests was large enough to completely compact the void out of the material. The pressure at complete void closer provided a good starting point for estimating P_s. By adjusting P_s and N in the P-Alpha equation (3), the curve was fit in line with the adobe laboratory data and compaction curve. When aligning the P-Alpha curve the main objective was to match the areas under the curves showing same amount of work being accomplished during compression of the adobe. Figure 6 shows the P-Alpha and compaction curves aligned to the lab data. From the lab data, P_s was approximated at 460 MPa at a lock-up density (ρ_s) of 2458 kg/m^3.

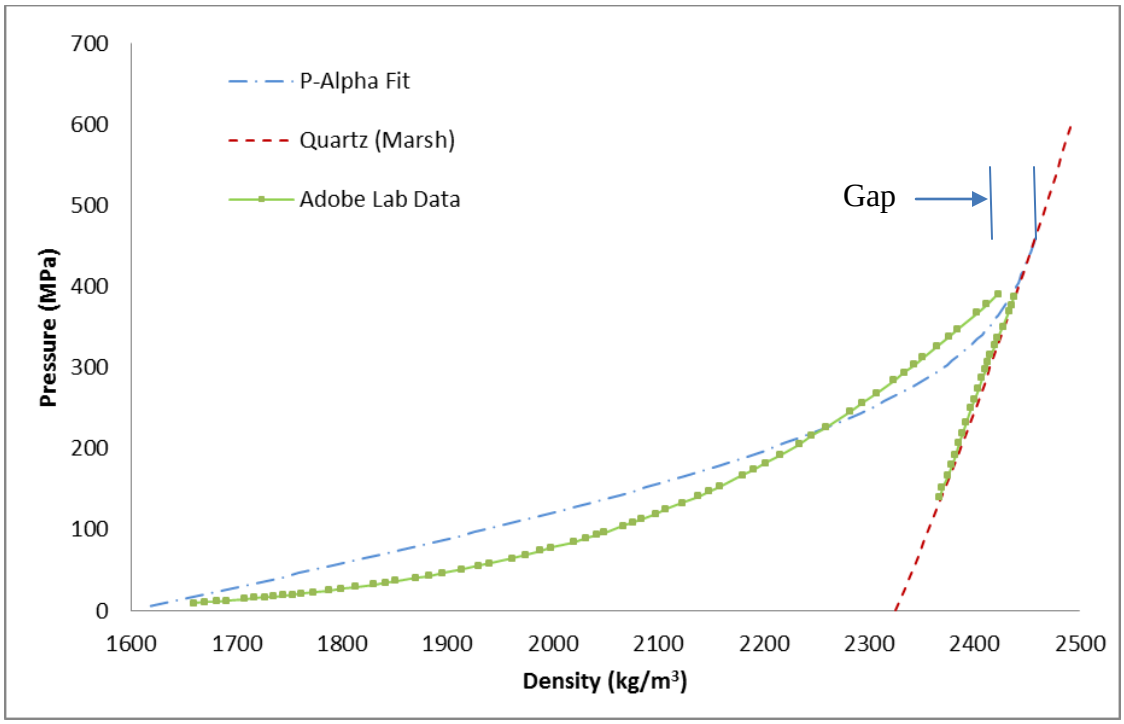

Figure 6: Pressure versus Density Computational P-Alpha Curve aligned to Test Data and Quartz Compaction Curve

Elastic Plastic Parameters (Deviatoric)

There are 4 elastic plastic parameters needed for the strength model; yield strength, yield strength at zero pressure (YZero), poisson's ratio, and slope of the yield surface as a function of pressure (DYDP). To find the parameters, the shear and failure data (figure 7) from the compression tests provided by ERDC 2008 study were needed. Extrapolating data from figure 7 and using equations 6 and 7 provided by the ERDC, the yield stress was calculated as a function of mean normal stress. In Equation 6, the principal stress difference (q) equals the axial stress (σ_a) minus the radial stress (σ_r). The mean normal stress ($P_{Mean\ Normal}$) is defined in equation 7.

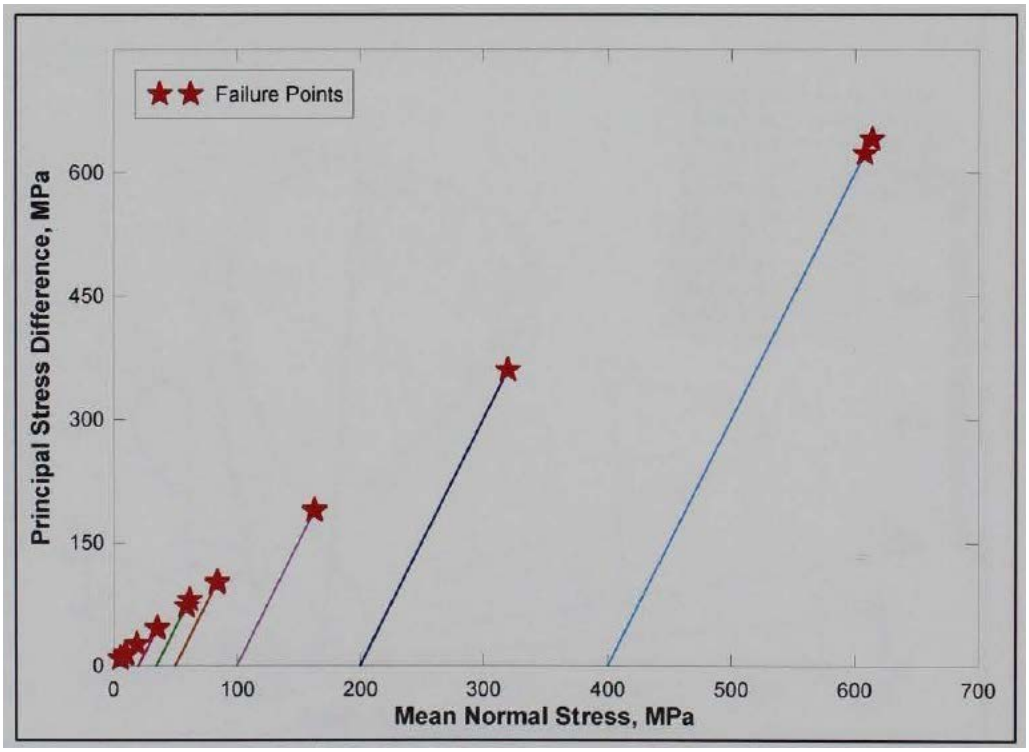

Figure 7: Shear Failure Test Data of Adobe Specimens Provided by ERDC (Williams et al, 2008)

$$q = \sigma_a - \sigma_r \qquad \text{Equation 66}$$

$$P_{Mean\ Normal} = \frac{\sigma_a + 2\sigma_r}{3} \qquad \text{Equation 77}$$

Figure 8 is the plot of the calculated yield stress versus mean normal stress extrapolated from figure 7. The slope and y-intercept of the yield stress versus the mean normal stress provided parameters for the deviatoric portion of the CTH model.

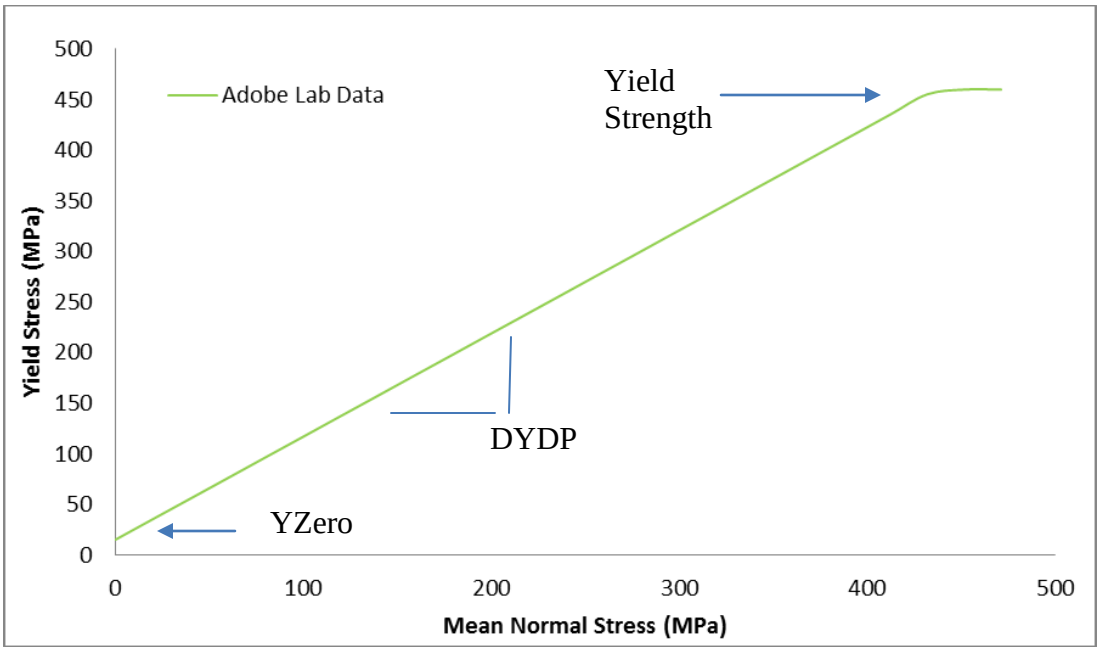

Figure 8: Yield Stress versus Mean Normal Stress of Adobe Test Data

Yield stress is shown to peak at 460 MPa (yield strength) approximated earlier from the P-Alpha curve fit. The yield strength at zero pressure computed at 15.3 MPa (y-intercept) and 1.019 is the slope of the of the line at zero pressure (DYDP) in figure 8. Poisson's Ratio (0.23), provided by ERDC was calculated from the bulk modulus (K=318 MPa) and shear modulus (G=209 MPa) of the adobe (equation 8).

$$Poisson's\ Ratio = \frac{3K - 2G}{2(3K + G)} \qquad \text{Equation 88}$$

Chapter 3

Problem Setup

The shock physics code CTH with adaptive mesh refinement was applied to model and simulate the cratering of a sphere projectile into adobe. All GEO simulations were two dimensional cylindrical (2-DC) with young's reconstruction algorithm convection input (SMYRA) and volume averaged yield strength normalized by the sum of the volume fractions of the materials that can support shear (Mix=3). The level of refinement for the adaptive mesh uniformly sectioned the problem to 0.16 by 0.16 mm blocks for any material above the initial density of the target. Figure 9, on the left is a two dimensional material plot of sphere projectile prior impacting adobe and on the right, a two dimensional density plot of a projectile deforming under hypervelocity impact with mesh refinement.

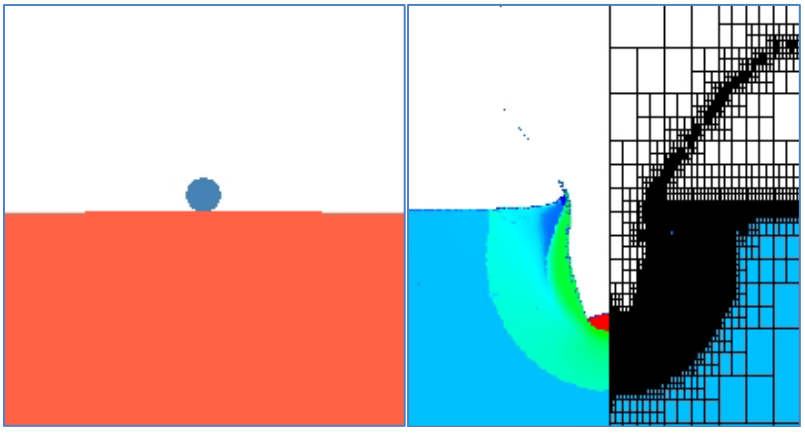

Figure 9: Left, Sphere Just Prior Impact Adobe. Right, Example of Refinement in Simulations using Density Indicator

Projectile Model

The projectile is a 1.35 cm diameter steel sphere ranging in impact velocities from 300 m/s to 2000 m/s into the adobe target. Steel was modeled with user defined MGR EOS material parameters for 4340 steel, at density 7.85 g/cm^3 and sound speed of 3574 m/s. Johnson Cook viscoplastic strength and Johnson Cook fracture models for 4340 steel were used in the elastic plastic section.

Target Material Model

The target is a 70 cm by 16 cm, two dimensional adobe model with boundaries set to simulate a semi-infinite target material. Adobe was modeled with a user defined MGR combined with P-Alpha EOS parameters from the earlier computations of solid density (ρ_o) at 2.325 g/cm^3, porous density (ρ_{oo}) at 1.6 g/cm^3, bulk sound speed at 1746 m/s, compaction pressure at 460 MPa, and constant "*N*" at 3.0. Elastic plastic parameters were user defined GEO model inputs of yield strength (460 MPa), yield strength at zero pressure (15.3 MPa) and yield surface slope (1.019) computed from shear failure data. Poisson's ratio was provided by ERDC at 0.23.

Chapter 4

Simulation Results

Penetration Depth and Impact Velocity

In the work done by Heine, there wasn't much explanation on the characteristics of the adobe used but Heine did notice in the research the penetration behavior of steel spheres into adobe was captured by Stokes law, where drag coefficient is inversely proportional to the Reynolds number. This behavior within the linear region (Stokes region) is true prior to the impact velocity being high enough to deform the projectile. Post projectile deformation depth will actually decrease as the impact velocity increases, per the contact surface area of the projectile increasing. Meyer's HJC model was also able to replicate the same characteristic of a linear relationship between depth and impact velocity prior to projectile deformation.

The new adobe model (GEO) in CTH achieved comparable results to Meyer's HJC model and Heine's test data. Figure 9 shows normalized depth versus impact velocity of Heine's test data, Meyer's HJC simulations and the GEO simulations. Normalized depth is the penetrator depth (P) divided by projectile diameter (D) and density of the projectile (ρ_p). The adobe model used in the GEO simulations is different than both Heine's and Meyer's model, but the same characteristics showed up for all three. There is a linear relationship of projectile depth and impact velocity for all three data sets prior to projectile deformation. As the slope of depth versus impact velocity decreases, deformation of the projectile increases referred to as the

transition point, shown in figure 10 as the horizontal dashed lines. Appendix A shows two dimensional material and density plots of craters formed from impact velocities ranging from 600 m/s to 2000 m/s. As the impact velocity increases past 1400 m/s the penetrator is noticeably deforming and crater width is increasing.

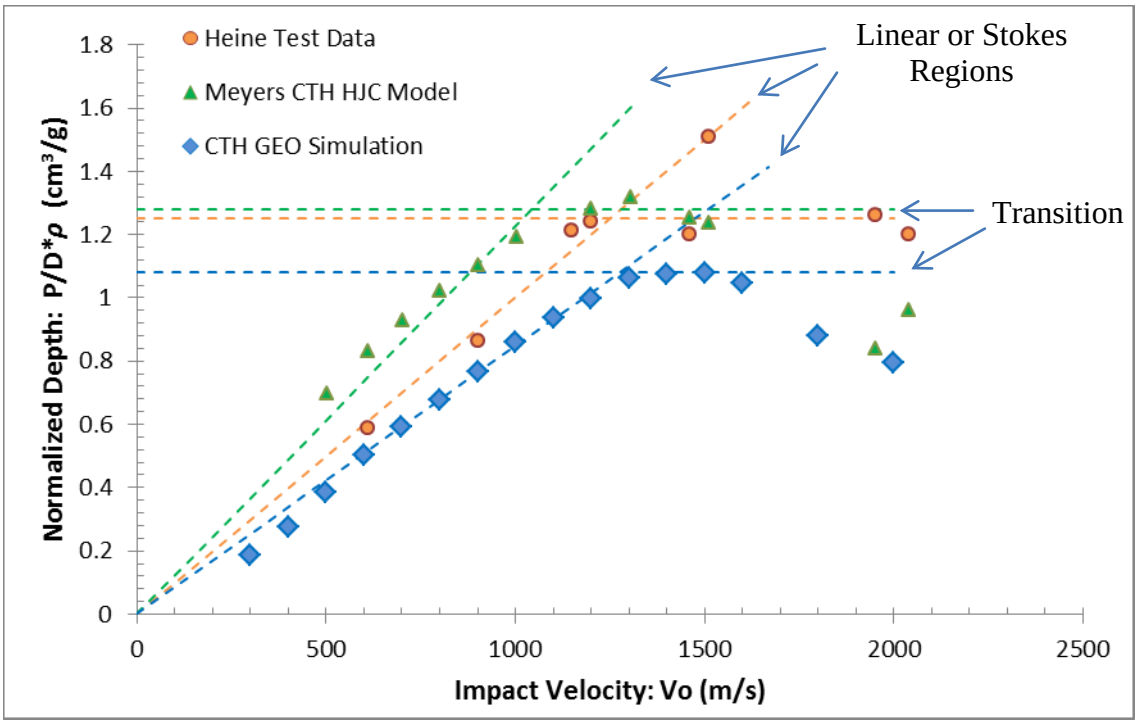

Figure 10: Normalized Penetrator Depth versus Impact Velocity Comparing Test and Computational Data of Adobe Penetrations

The linear relationship between penetrator depth and impact velocity was initially described by Heine using Newton's second law ($\vec{F} = m\dot{a}$) and the coefficient of drag equation (equation 9). The coefficient of drag (C_d) is described as the force of drag (F_d) on the projectile, divided by target density (ρ_T), projectile velocity (v_o) and projectile diameter (D).

$$C_d = \frac{8 \cdot F_d}{\rho_T \cdot {v_0}^2 \cdot \pi \cdot D^2} \qquad \text{Equation 99}$$

By introducing a new constant *A*, the coefficient of drag can be expressed as (C_d=*A*/*v*). Refer to Heine[5] for the derivation of equation 10. The linear region can now be expressed in equation 11, where constant *A* is a function of penetration depth (*P*), projectile diameter (*D*), projectile density (ρ_P), target material density (ρ_T), and impact velocity (υ_o). The same equation was used for describing the linear regions of HJC data and GEO data in figure 9.

$$\frac{P}{D} \cdot \frac{1}{\rho_P} = \frac{4}{3 \cdot \rho_T \cdot A} v_0 = const \cdot v_0 \qquad \text{Equation 1010}$$

$$\frac{1}{A} = \frac{3 \cdot P \cdot \rho_T}{4 \cdot v_0 \cdot \rho_P \cdot D} \qquad \text{Equation 1111}$$

Comparing the three different data plots, it was easy to notice the differences in slope of the Stokes region and points of transition. Although we don't know much about Heine's adobe, the correlation of Meyer's model to the GEO model with a steeper slope and higher transition point is believed to be linked to differences in key parameters between the models. Table 1 shows key parameter differences in the adobe targets between the HJC and GEO models.

Table 1: Comparison of HJC Inputs and GEO Inputs

Parameters	**HJC Model Inputs**	**GEO Model Inputs**
Initial Density: ρ_{oo} (g/cm^3)	1.8	1.6
Solid Density: ρ_o (g/cm^3)	2.51	2.325
Sound Speed: C_s (m/s)	1070	1746
Compaction Pressure: P_s (MPa)	20	460

Shown in both table 1 and figure 9, even small differences in key parameters can have significant effects on projectile depth and transition of projectile deformation. The next section will look at key parameter adjustment and the sensitivity those parameters associated with adobe cratering.

Adobe Parameter Sensitivity: Compaction and Yield Pressure

The GEO model is based upon few parameters to characterize crater depth and formation under high velocity impacts. By adjusting the few parameters, one at a time, the sensitivity of depth versus impact velocity can be analyzed. The three parameters adjusted, one at a time for the adobe model, were compaction pressure (P_s), yield strength, and initial density (ρ_{oo}).

The first parameters analyzed were the compaction and yield pressure of adobe. Figure 11 shows the penetrator depth versus impact velocity of the test data compared to three different GEO models of varying compaction pressure. Adjusting adobe compaction pressure from 230 MPa ($P_{s,Low}$) to 690 MPa ($P_{s,High}$), resulted in minimal changes to the depth of penetration. As shown earlier, the Stokes region and transition portions of the data still hold true when varying compaction pressure. These results show penetration depth to be fairly insensitive to changes in compaction pressure alone within the pressures shown.

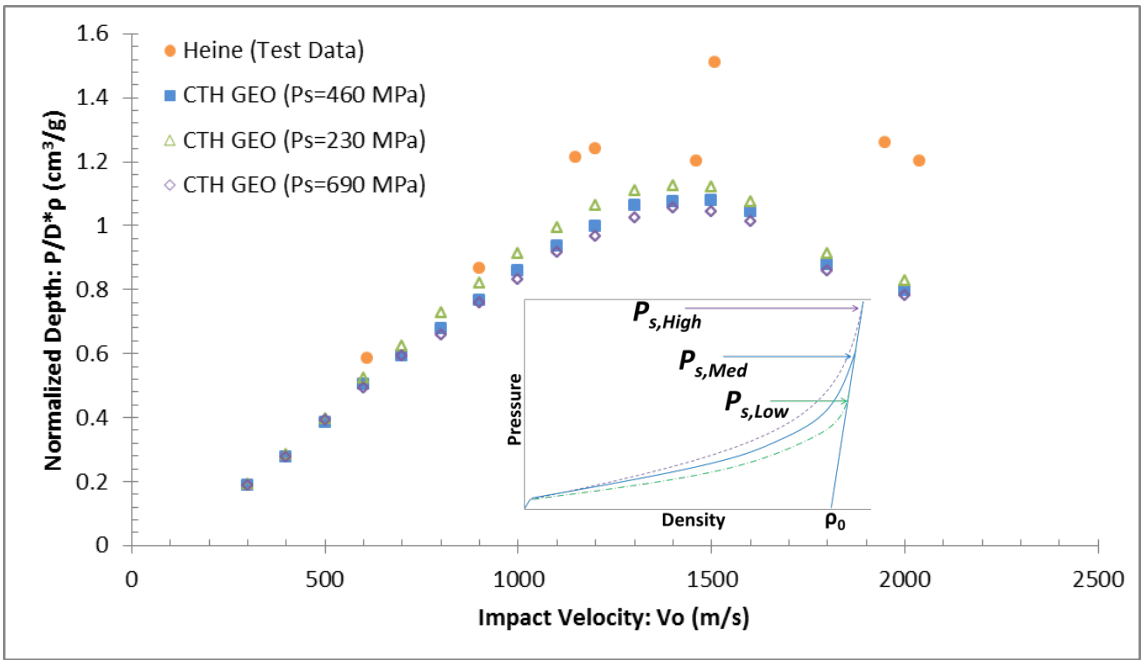

Figure 11: Normalized Depth versus Impact Velocity of Computational Data varying Adobe Compaction Pressure Compared to Test Data

Figure 12 shows the penetrator depth versus impact velocity of the test data compared to three different GEO models of varying yield strength. Adjusting adobe yield strength from 230 MPa (Low_{yield}) to 690 MPa ($High_{yield}$), resulted in minimal changes to the depth of penetration. As shown earlier, the Stokes region and transition of the data still hold true when varying yield strength. These results show penetration depth to be fairly insensitive to changes in yield strength alone within the pressures shown.

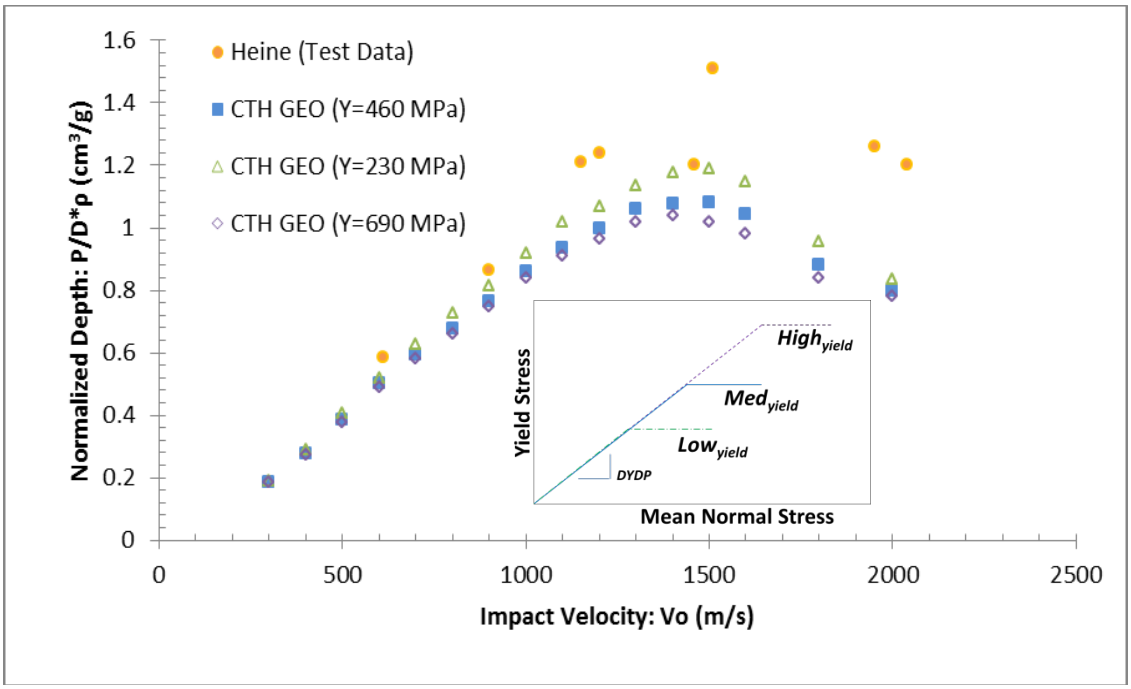

Figure 12: Normalized Depth versus Impact Velocity of Computational Data varying Adobe Yield Strength Compared to Test Data

By varying one parameter at a time at a constant impact velocity, the sensitivity associated with that parameter can be analyzed. Figure 13 analyses the correlation of penetrator depth to compaction pressure and yield strength of adobe at a constant impact velocity of 1.2 km/s. As the values of the yield strength and compaction pressure decrease beyond 200 MPa, the depth of penetration increases at a non-linear rate concluding the depth of penetration is more sensitive to the parameters at lower pressures.

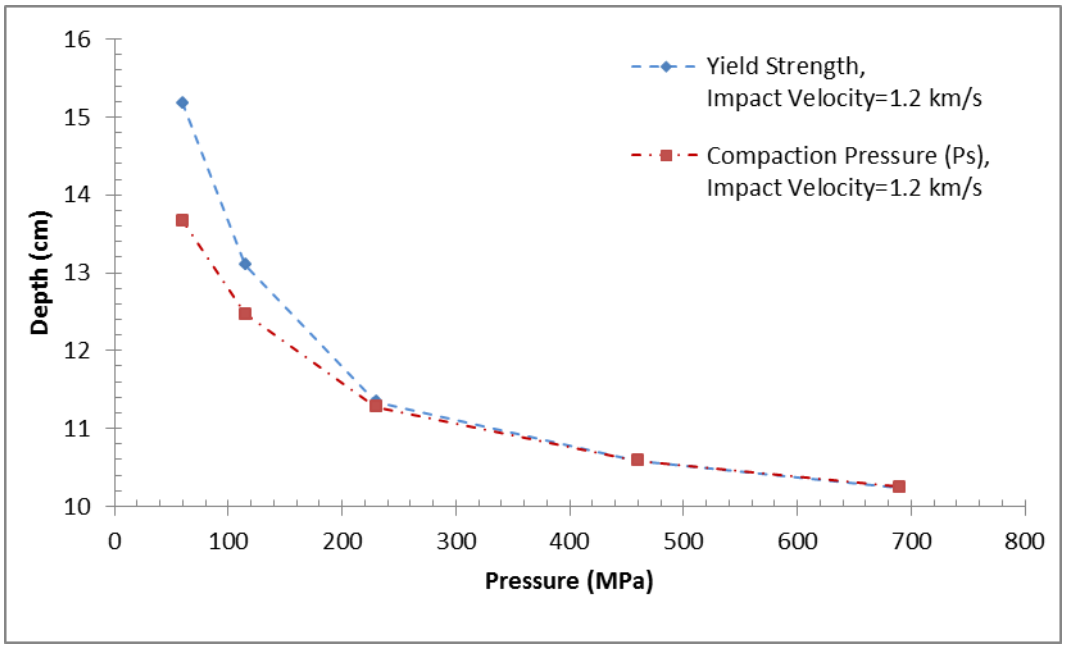

Figure 13: Penetrator Depth versus Impact Velocity of Computational Data varying Yield Strength and Compaction Pressures at Constant Velocity

Adobe Parameter Sensitivity: Initial Density

The third parameter under analysis is adobe initial density. Figure 14 shows the penetrator depth versus impact velocity of the test data compared to three different GEO models of varying adobe initial density. Adjusting initial density from 1.2 g/cm^3 (Low_{yield}) to 2.0 g/cm^3 ($High_{yield}$) resulted in large changes to the depth of penetration. As shown earlier, the Stokes region and transition of the data still hold true when varying initial density but when adjusting initial density from 1.6 g/cm^3 to 1.2 g/cm^{3}the slope of the Stokes region increased ~25%. Similar, the transition increased ~50% when adjusting initial density from 1.6 g/cm^3 to 1.2 g/cm^3. These results show that depth of penetration is relatively sensitive to initial density.

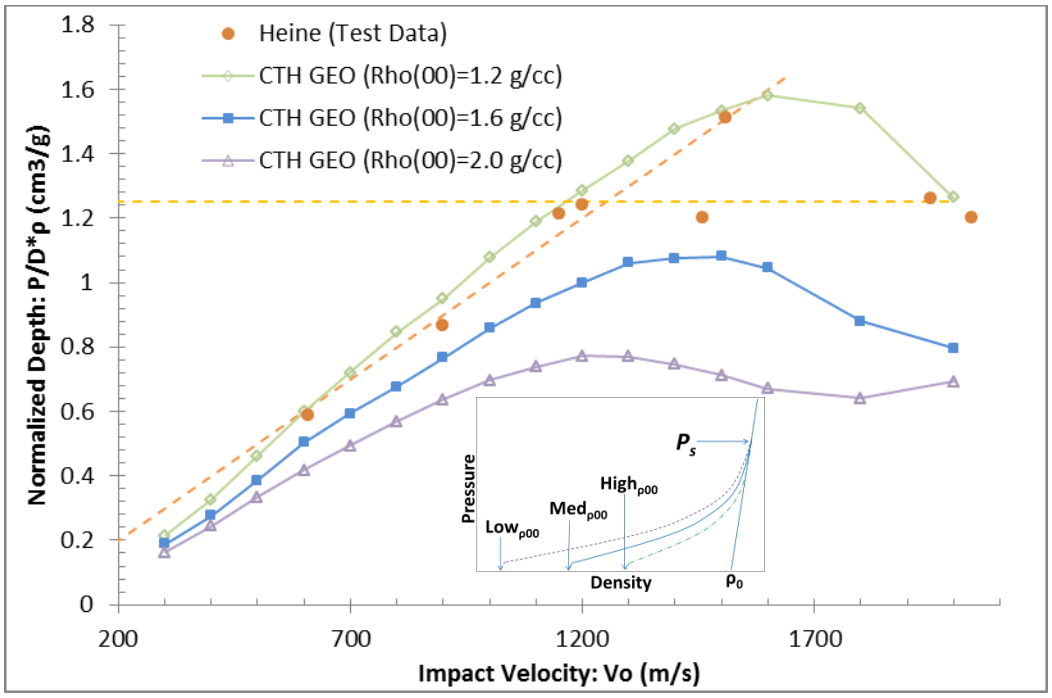

Figure 14: Normalized Depth versus Impact Velocity of Computational Data varying Adobe Initial Density Compared to Test Data

Figure 15 analyses the correlation of penetrator depth to adobe initial density at a constant impact velocity of 1.2 km/s. Varying initial density at constant impact velocity shows the sensitivity to depth of penetration from the parameter. As the initial density is varied from 2 g/cm^3 to 1.2 g/cm^3 the depth of penetration shows to be linear in respect to initial density.

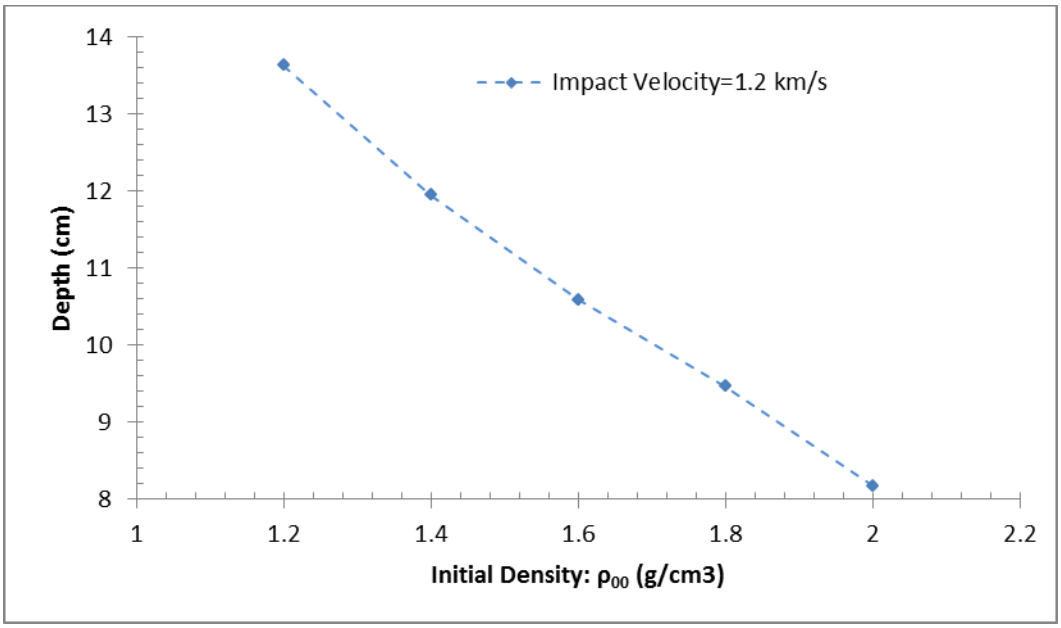

Figure 15: Penetrator Depth versus Density of Computational Data varying Initial Densities at Constant Impact Velocity

Aligning GEO simulation data to Heine's test data is accomplished by adjusting initial density. Equation 12 is derived by using the left side of equation 11 and setting Heine's parameters equal to the GEO parameters. To match GEO simulation data to the test data the initial target density was calculated at 1.37 g/cm^3 using equation 13. In equation 12 penetration depth (P) is divided by projectile diameter (D) and penetrator density (ρ_P).

$$\left\lfloor \frac{P}{D \cdot \rho_P} \right\rfloor_{GEO} = \left\lfloor \frac{P}{D \cdot \rho_P} \right\rfloor_{HEINE} \qquad \text{Equation 1212}$$

$$\lfloor \rho_T \rfloor_{GEO} = \frac{\lfloor \rho_T \cdot A \rfloor_{HEINE}}{\lfloor A \rfloor_{GEO}} \qquad \text{Equation 1313}$$

Figure 16 shows GEO simulations with the adjusted initial target density to match Heine's experimental depth of penetrations in adobe. At lower velocities below 1150 m/s, the normalized depth of penetration is comparable to the test data. The differences in normalized depth between the GEO simulations and test data increase at impact velocity of 1200 m/s and beyond. Not knowing the error in the test data, it is hard to determine how close the simulated results are to the actual physics of the penetrating adobe in Heine's experiments.

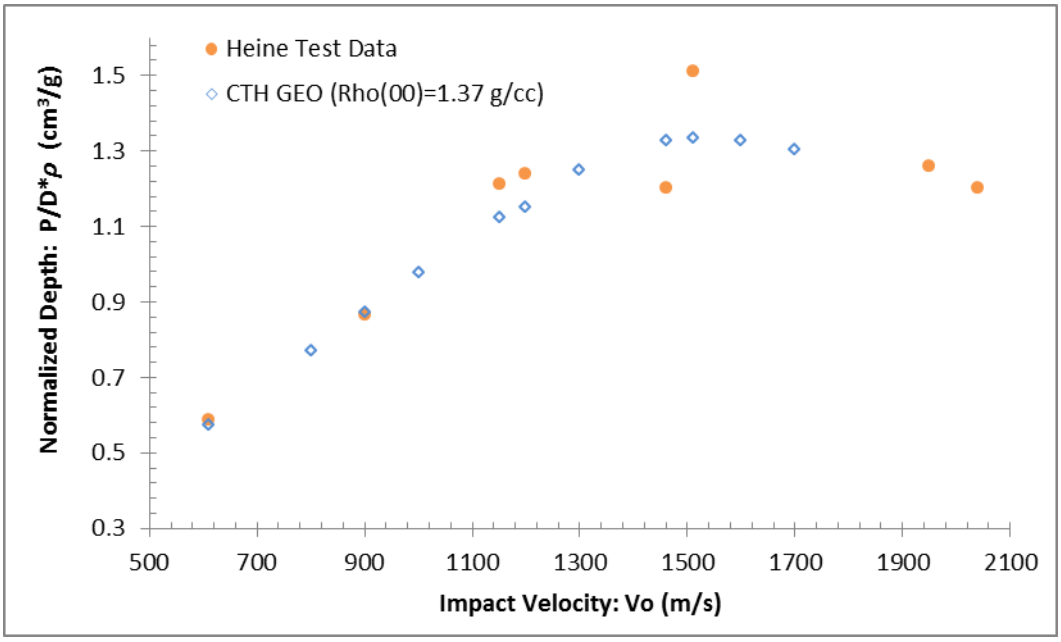

Figure 16: Normalized Depth versus Impact Velocity of Computational Data Approximately Matched to Test Data by vary of Initial Density

Adjusting one parameter at a time demonstrated the sensitivity to depth of penetration from each parameter. The adjustment of multiple parameters can show a compound effect on the outcome as described in the next section.

Water Content in Adobe

The model of adding water to adobe can be accomplished by assuming in dry porous adobe, no water (or very little) is present but when water is added the volume of air occupying the space is replaced by water. Figure 17 is an example of adding water to a constant volume of water, air and adobe grains.

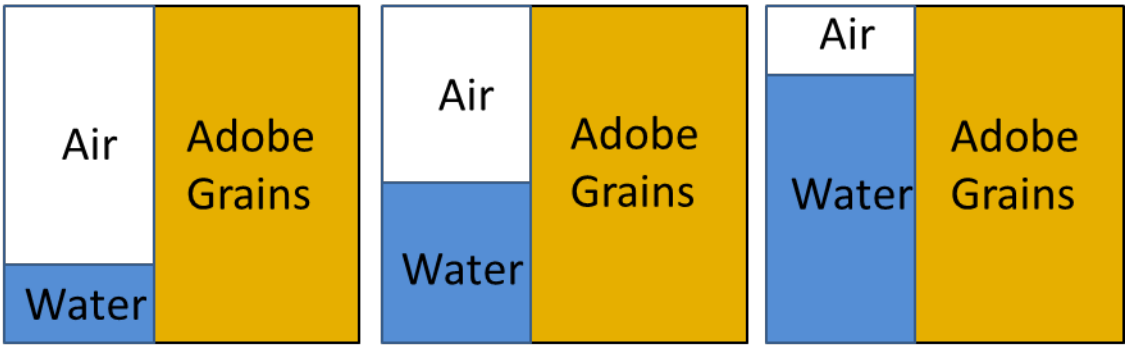

Figure 17: Example of Water Added to Adobe at Constant Volume

Equation 14 describes the solid density (ρ_o) of the adobe in terms air ration (ϕ_{air}), water ratio (ϕ_{water}), solid adobe ratio (ϕ_o), adobe initial density (ρ_{oo}), density of air (ρ_{air}) and density of water (ρ_{water}). The solid density of adobe is functions of water ratio by keeping all other variable in equation 14 constant. The adobe solid density will decrease linearly with the increase of water.

$$\rho_o = \frac{\rho_{oo} - \phi_{air}\rho_{air} - \phi_{water}\rho_{water}}{\phi_{air}} \qquad \text{Equation 1414}$$

Figure 18 is past research of stress versus density of soils with varying water content conducted by Holcomb in 2005. By increasing the amount of water in the soil the density at which the soil locks up also decreases.

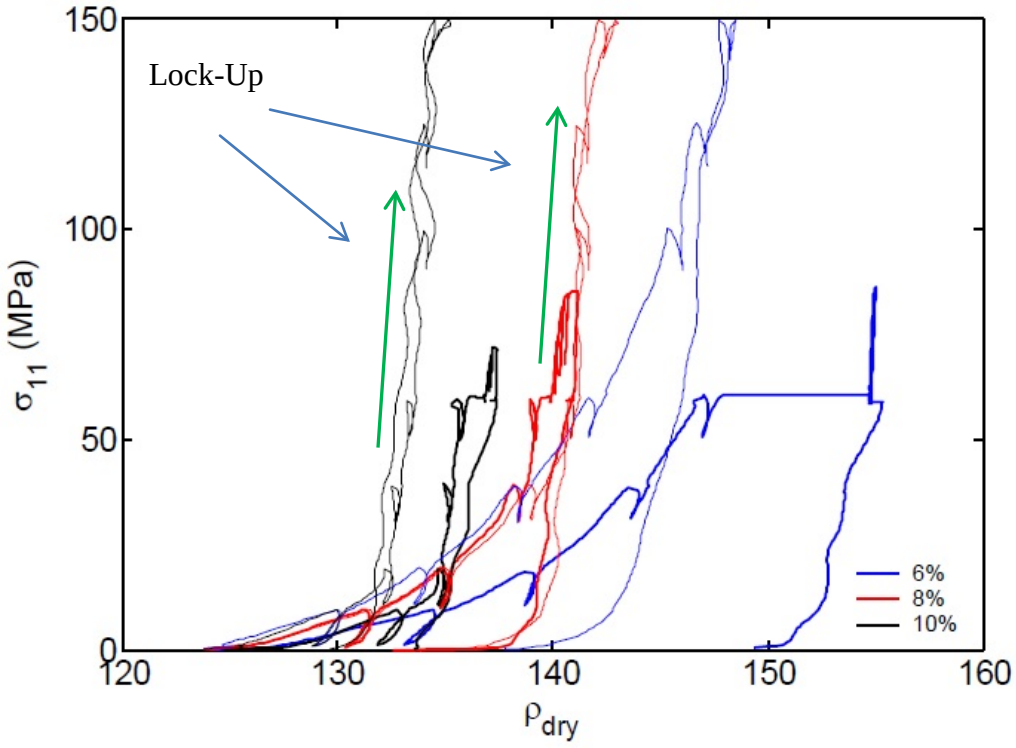

Figure 18: Stress versus Density Test Data of Increasing Water Content in Soil

The model of adding water to adobe can first be expressed through equation 14, where the increase of water decreases the adobe solid density. Figure 19 is an example of adjusting solid density on the P-Alpha curve and resulting adjustments. As shown, decreasing the adobe solid density (ρ_{o1} to ρ_{o3}) results in decreasing the compaction pressure (P_{s1} to P_{s2}) and yield strength ($Yield_1$ *to* $Yield_3$) of the adobe.

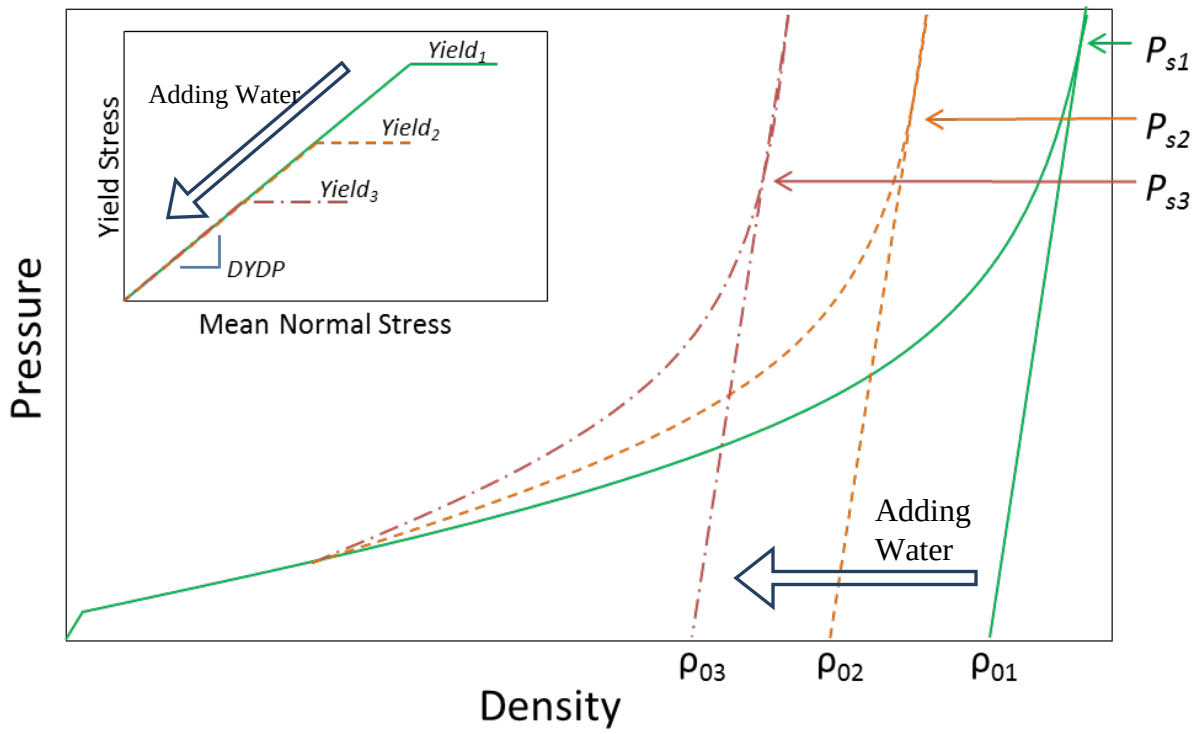

Figure 19: Example of P-Alpha and Yield Adjustments with Addition of Water to Adobe

Figures 20 and 21 show the increase of penetration depth and crater volume with increasing water content in adobe for several impact velocities. This effect is not linear for either figure but a second order effect where depth of penetration and crater volume increases faster than the increase of water added to adobe. In figure 20 as impact velocity increases from 1.2 km/s to 1.46 km/s the depth of penetration increases but as the impact velocity increases from 1.46 km/s to 1.8 km/s the penetration depth dramatically decreased. The decrease in penetration depth is related to the increase of penetrator deformation. In figure 21 crater volume increases with water added to adobe. As the impact velocity is increased from 1.2 km/s through 1.8 km/s the crater volume is consistently higher for each percent of water added.

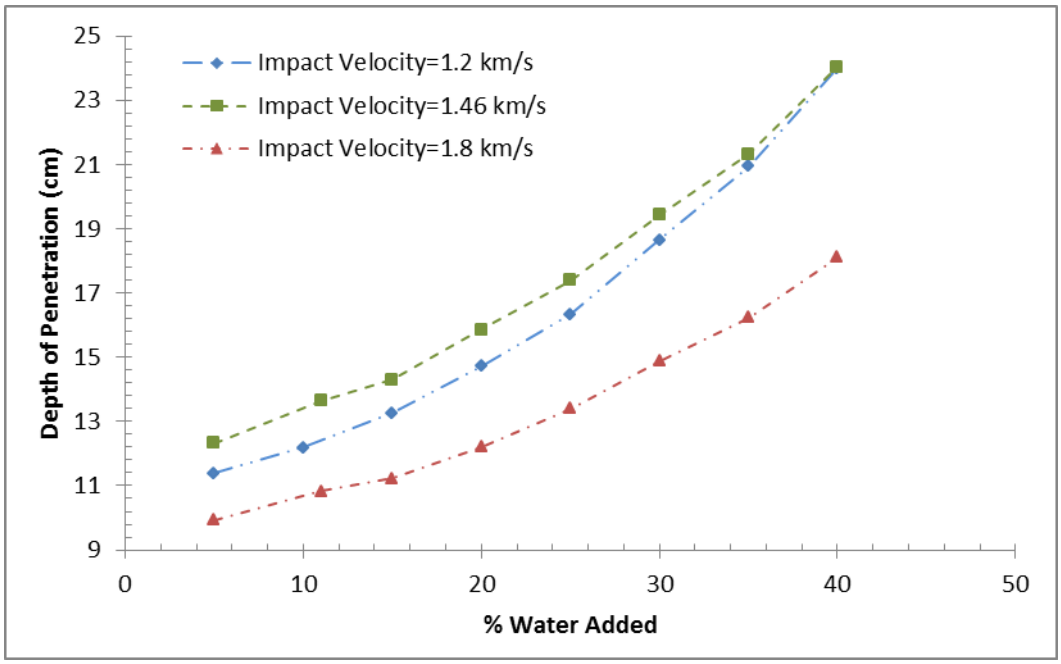

Figure 20: Depth of Penetration versus Percent Water Added to Adobe Computational Data

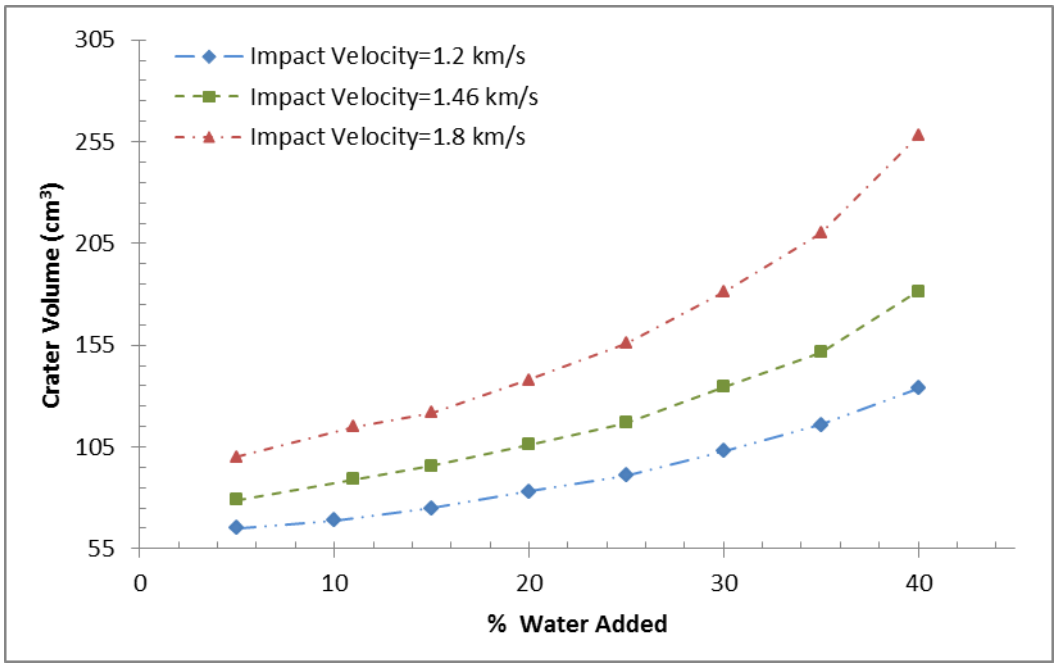

Figure 21: Crater Volume versus Percent Water Added to Adobe Computational Data

Appendix B shows two dimensional craters formed from adding water to adobe at constant impact velocity of 1.2 km/s. Shown in the crater formation, as more water is added to the target adobe the crater continues to increase in width and depth per the water decreasing the shear strength. Table 2 shows the correlation of penetrator depth and crater volume to percent of water added.

Table 2: Computational Results of Increasing Water Content to Adobe

Impact Velocity (m/s)	Depth of Penetration (cm)	Crater Volume ($cm^{3)}$	% of Water Added to Adobe
1200	11.39	65	5
1200	12.19	69	10
1200	13.27	75	15
1200	14.73	83	20
1200	16.34	91	25
1200	18.65	103	30
1200	20.95	116	35
1200	24.00	134	40
1460	12.32	79	5
1460	13.64	89	10
1460	14.31	96	15
1460	15.85	106	20
1460	17.40	117	25
1460	19.44	134	30
1460	21.33	152	35
1460	24.04	181	40
1800	9.93	100	5
1800	10.82	115	10
1800	11.23	122	15
1800	12.21	138	20
1800	13.41	156	25
1800	14.89	181	30
1800	16.23	210	35
1800	18.11	258	40

Figure 22 is normalized depth versus impact velocity of GEO simulations with increasing water content in adobe compared to the test data. Increasing the water content by 5% to the

adobe yielded an increase of ~10% in normalized penetration depth at the upper end of the Stokes region. Using figure 20 and setting a second order polynomial trend line to the 1.2 km/s data, it was calculated that adding 11% percent water to the adobe aligned the GEO simulations to the test data. Although the GEO simulation data does not exactly represent the test data, this simplistic approach yielded a reasonable comparison given the unknown error in the test data and the initial water content of the adobe under test. Appendix C lists the parameters adjusted for each sensitivity study and the parameters adjusted to replicate the addition of water to adobe.

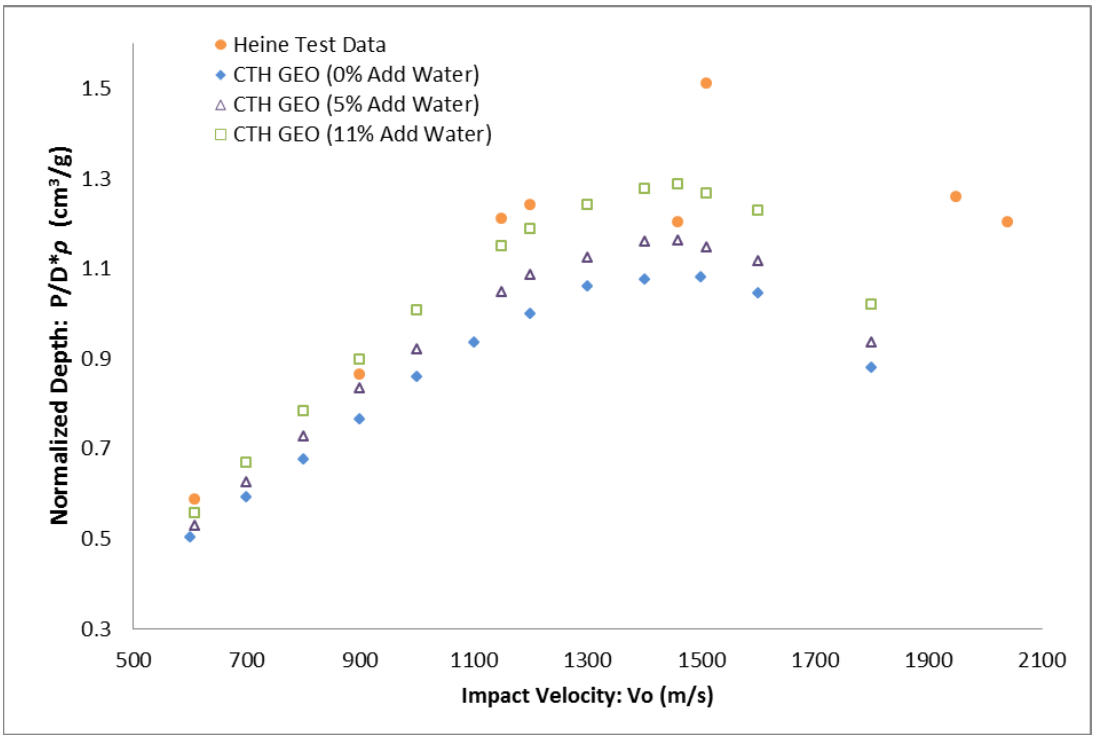

Figure 22: Normalized Depth of Penetration versus Impact Velocity of Computational Data of varying Water Content Compared to Test Data

Chapter 5

Summary and Discussion

It should be possible to explain the laws of physics to a barmaid

—Albert Einstein

Previous simulations used the EOS and yield surface of adobe to fit a HJC model in CTH. This work represented an approach to develop a computational model to predict steel sphere and rod penetrator depth data acquired by penetrating a different adobe brick material characterized by Heine. Unfortunately, limited characterization data were provided by Heine, and the exact adobe material used by Heine was unable to be modeled. Hence, the HJC model developed by Meyers was representative of adobe, combining EOS and strength parameters of various types of adobe and high pressure compression data of geologic materials from Marsh.

The new simplistic adobe model was shown to replicate the same features within Heine's test data and Meyer's HJC model. There is a linear correlation to depth and impact velocity of the projectile at lower velocities which is captured by Stokes law, where the penetrator depth versus impact velocity is proportional to $1/A$ (Stokes Region). Following the Stokes region, there is a transition where the penetrator depth is constant with increasing impact velocity. This transition region is shown to be related to the deformation of the projectile, also determined in both Heine's experiments and Meyer's HJC model.

The analysis of three key parameters (compaction pressure, yield strength, and adobe initial density) showed that varying some parameters is more sensitive in effecting depths of

penetrations. Varying of compaction pressure or yield strength of the target material from 230 MPa to 690 MPa showed to have a minimal effect (5%-10% delta) on the penetration depth at a constant velocity. Decreasing the compaction pressure or yield strength below 200 MPa, showed an exponential effect on penetration depth. The varying of adobe initial density showed to have large effects on projectile depth and slope of the Stokes region. Decreasing the adobe initial density from 1.6 g/cm^3 to 1.2 g/cm^3 increased the slope of the Stokes region by 25% and the transition by ~50%. It was found the adobe initial density is linearly, inversely proportional to penetrator depth. By setting the parameters equal to each other as shown in equation 12, a calculated initial density was found to replicate the test data. The GEO simulation data reasonably replicated the test data using this very simple approach.

Adjusting more than one key parameter showed to have a compound effect on projectile depth and crater volume. Simulating the addition of water resulted in varying the parameters adobe solid density, compaction pressure and yield strength. By adding water, the GEO simulations showed increases in crater volume and penetration depths within the Stokes regions. Applying a second order polynomial to the sensitivity study in figure 20, the amount water needed to replicate the test data was found. This simplistic approach of adjusting water content was able to reasonably match the test data.

This study concludes test data, with few material characteristics and unknown error, can reasonably be validated by adjusting a few key parameters with a simple MGR / P-Alpha model combined with GEO strength model.

Future Work

For future work, it would be beneficial to acquire adobe specimens from several vendors with varying water content, and conduct static compression tests combined with high velocity

impact studies. The idea is to see the natural variation of adobe from different locations and water content to help fully characterized the behavior of adobe under high pressures.

Appendix A

Crater Formation of Original GEO Simulations

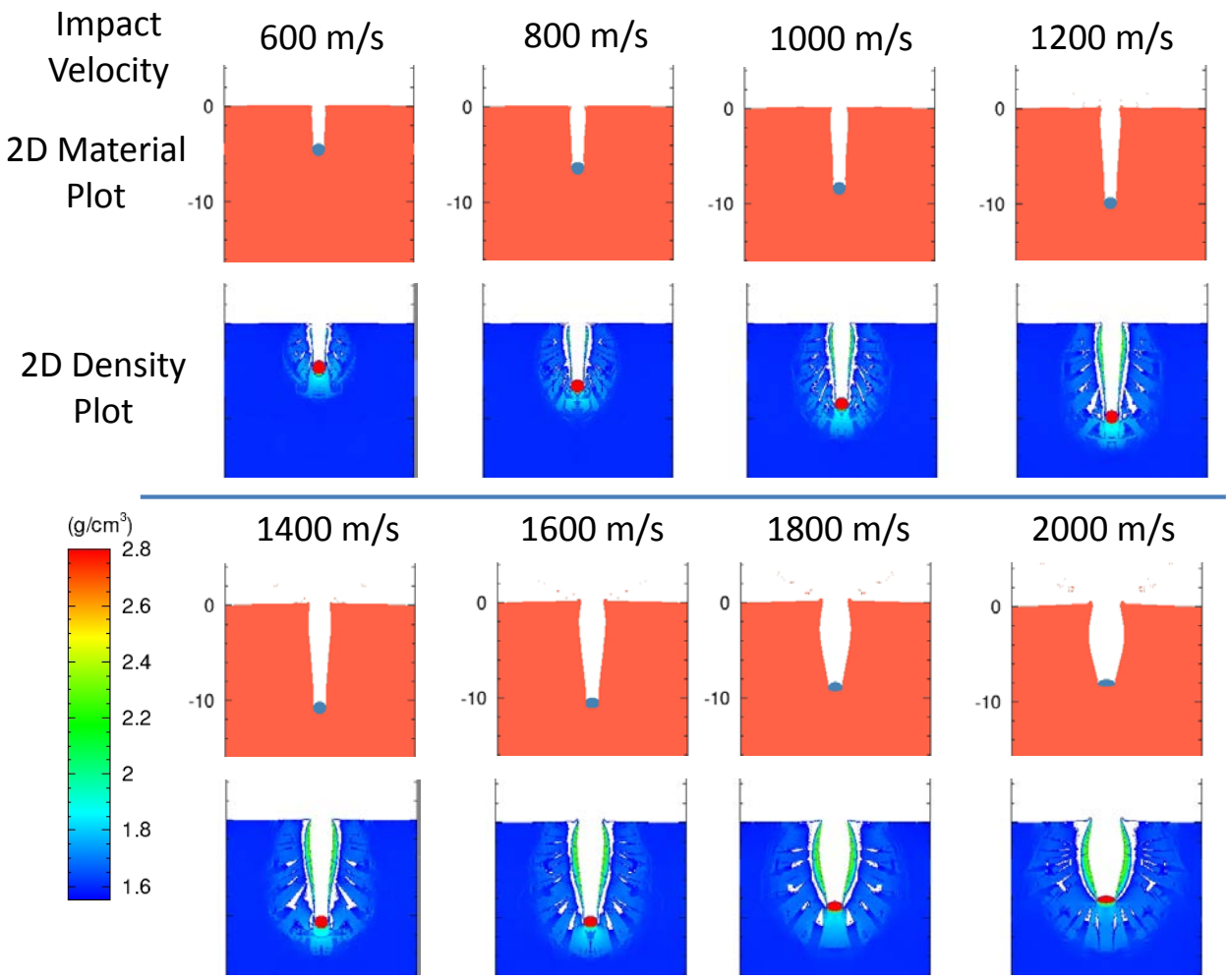

Appendix B

Addition of Water to Adobe: Impact Velocity=1.2 km/s

%Water=0%

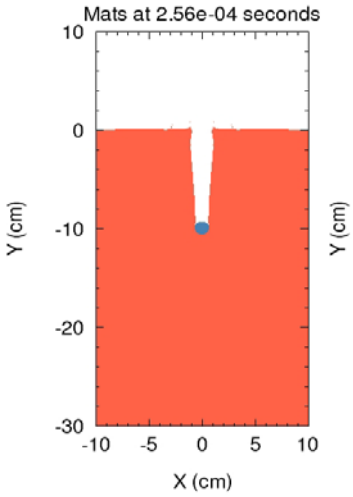

%Water=10%

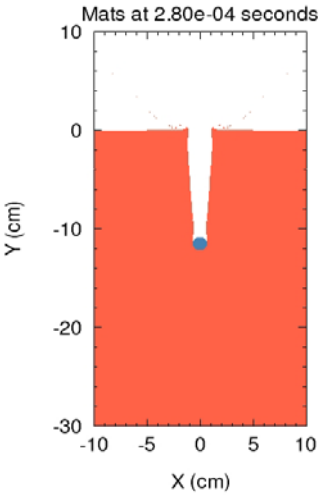

%Water=20%

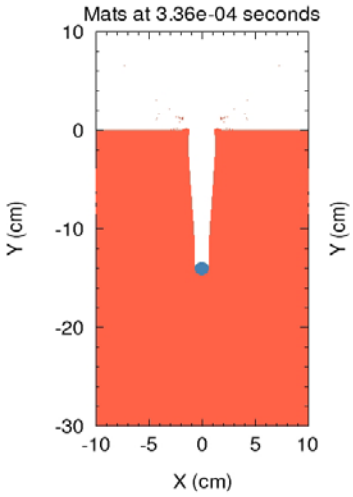

%Water=30%

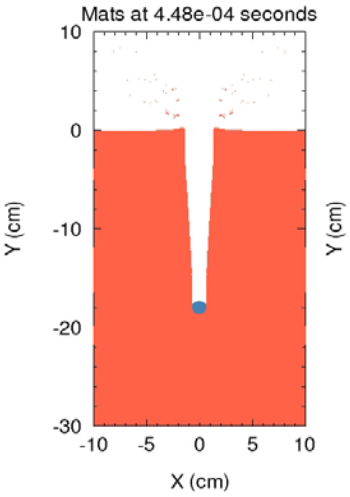

%Water=40%

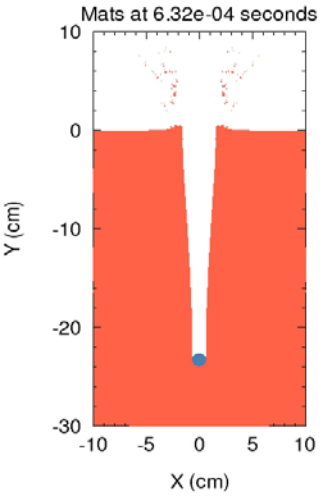

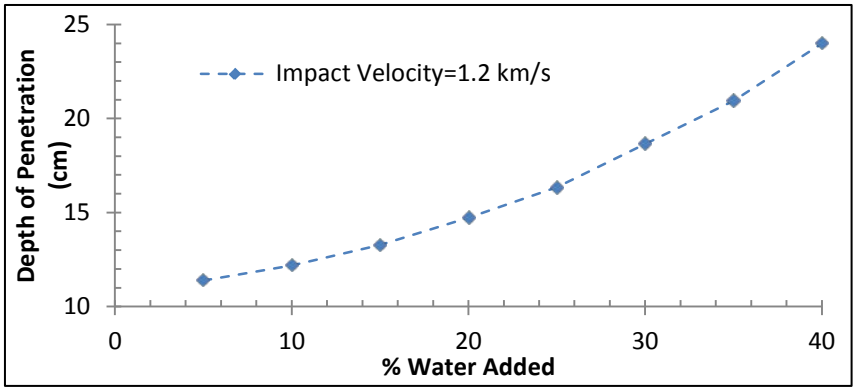

Appendix C

Parameter Adjustments

Property	Symbol	Unit	Original GEO Simulation	Vary Compaction Pressure	Vary Yield Strength	Vary Initial Porous Density	Addition of Water to Adobe
Initial Porous Density	ρ_{00}	g/cm^3	1.6	1.6	1.6	High: 2.0 Med: 1.6 Low: 1.2	1.6
Grain Density	ρ_0	g/cm^3	2.325	2.325	2.325	2.325	0%: 2.325 5%: 2.252 11%: 2.148
Sound Speed	*C*	m/s	1746	1746	1746	1746	1746
Shock Constant	*s*	-	1.63	1.63	1.63	1.63	1.63
Compaction Pressure	P_s	MPa	460	High: 690 Med: 460 Low: 230	460	460	0%: 460 5%: 300 11%: 185
Elastic Pressure	P_E	MPa	5.0	5.0	5.0	5.0	5.0
P-Alpha PWR	*N*	-	3	3	3	3	0%: 3 5%: 2.4 11%: 2.4
Yield Strength	*Yield*	MPa	460	460	High: 690 Med: 460 Low: 230	460	0%: 460 5%: 300 11%: 185
Yield Strength at Zero Pressure	*YZero*	MPa	15.3	15.3	15.3	15.3	15.3
Slope at Zero Pressure	*DYDP*	-	1.019	1.019	1.019	1.019	1.019

Glossary

ARL	Army Research Laboratory
CTH	Sandia Shock Physics Code
DAF	Department of the Air Force
DoD	Department of Defense
DOE	Department of Energy
DYDP	Slope at Zero Pressure
EOS	Equation of State
ERDC GSL	U.S. Army Corps of Engineers Engineer Research and Development Center, Geotechnical Structures Laboratory
GEO	Geological Surface Yield
HJC	Holmquist Johnson Cook
MGR	Mie-Grüneisen Analytical Model
MPa	Mega Pascal
P-Alpha	Pressure versus Alpha
YZero	Pressure at Y-Intercept

References

1. Beatty, H.B; Graham, S.S; Moxley, R.E; Akers, S.A.; Reed, P.A; Laboratory Characterization of Adobe (Scottsdale); ERDC/GSL TR-12-26; U.S. Army Corps of Engineers Engineering Research and Development Center, Geotechnical and Structures Laboratory; Vicksburg, MS, 2012

2. Brannon, R. M.; Fossum, A. F.; Strack, O. E.; KAYENTA: Theory and User's Guide; SAND2009-2282; Sandia National Laboratories; Albuquerque NM, 2009

3. Cooper, P. W. Explosives Engineering. Wiley-VCH 1996. Chapter 16-18 pp. 179-222

4. Crawford, D.A.; Brundage, A.L. "*CTH User's Manual and Input Instructions*" CTH Development Projects, Sandia National Laboratories; Albuquerque, NM, 2012

5. Heine, A.; Weber, K. E; Wickert, M.; Experimental Investigation of the Penetration and Perforation of Building Materials by Projectiles. Proceedings of the 26th International Symposium on Ballistics, Miami, FL, 12-16 September 2011; National Defense Industrial Association; Arlington VA

6. Kerley, G. I. CTH Equation of State Package: Porosity and Reactive Burn Models; SAND92-0553; Sandia National Laboratories; Albuquerque NM, 1992

7. Marsh, S. P; Mader, C. L.; Gibbs, T. R. "*Los Alamos Scientific Laboratory Shock Hugoniot Data*" Los Alamos Series on Dynamic Material Properties; Los Alamos National Laboratories; Los Alamos, NM 1980

8. Meyer, C. Modeling and Simulation of Adobe Penetration; ARL-TR-6329; U.S. Army Research Laboratory; Aberdeen Proving Ground, MD, 2013

9. Williams, E. M.; Aker, S.A.; Reed, P.A. Laboratory Characterization of Adobe; ERDC/GSL TR-08-11; U.S. Army Corps of Engineers Engineering Research and Development Center, Geotechnical and Structures Laboratory; Vicksburg, MS, 2008